The 4π k_z periodicity in photoemission from graphite

Fumihiko Matsui,[1,*] Hiroaki Nishikawa,[1] Hiroshi Daimon,[1] Matthias Muntwiler,[2] Masaru Takizawa,[3]
Hidetoshi Namba,[3] and Thomas Greber[4]

[1]*Graduate School of Materials Science, Nara Institute of Science and Technology, 8916-5, Takayama, Ikoma, Nara 630-0192, Japan*
[2]*Paul Scherrer Institut, CH-5232 Villigen, Switzerland*
[3]*Ritsumeikan University, 1-1-1 Nojihigashi, Kusatsu, Shiga 525-8577, Japan*
[4]*Physik-Institut, Universität Zürich, CH-8057 Zürich, Switzerland*

The valence band dispersion of the graphite π band along the k_z axis was measured using a sequence of photon energies between 60 and 230 eV. The interlayer interaction induces the well-known splitting of the π band into two, a lower binding energy band π_L and a higher binding energy band π_H. However, in the photoelectron spectra, the bands π_L and π_H appeared alternatively in the Brillouin zones along the k_z direction. As a result, a 4π-periodic oscillation in the binding energy as a function of photon energy was observed for the π band dispersion. This is explained by considering the constructive and destructive interference of p_z orbitals within the unit cell, called the *photoelectron structure factor*. We derived the analytic expression of the photoelectron structure factor for graphite. The resonance integrals of the p_z orbitals were determined for the in-plane and interlayer. Furthermore, the inner potential of graphite from the vacuum level was determined to be 17.17 eV.

I. INTRODUCTION

Photoelectron spectroscopy is a powerful technique for the investigation of the electronic structure of solids and surfaces. Photoelectron energy distribution curves for valence bands and core levels reflect the density of states and composition, respectively. The behaviors of valence electrons and the interference of photoelectrons appear as band dispersions and photoelectron diffraction patterns, respectively, in photoelectron intensity distributions in momentum space. Using the laws of energy and momentum conservation in the photoemission process, the valence band structure can be measured directly and a rich variety of information on the electronic structure of solids can be obtained.

Furthermore, the transition matrix elements affect the intensity of the photoelectron. In the case of linearly polarized excitation, the symmetry relation in the photoelectron excitation process also appears as the angular distribution from atomic orbital (ADAO) [1,2], which is used to distinguish the atomic orbitals constituting the valence band dispersion. Another important effect in angular distribution is the photoelectron structure factor (PSF) [2–6], which originates from the interference among photoelectron waves from individual atoms. Daimon *et al.* introduced the concept of PSF and succeeded in explaining the difference in the graphite π band intensity for the first and the second Brillouin zones (BZs) in the k_{xy} plane [2]. The phase of each atomic orbital wave function which determines the bonding character of the valence band dispersion can be accessed through the PSF observed as an intensity disparity among different BZs.

Here, we investigated PSF along the k_z axis of the layered material, graphite, which is important for the understanding of the interlayer interaction, but has not been studied well so far. The electronic structure of graphite has been studied extensively by angle-resolved photoelectron spectroscopy [2–24], inverse photoelectron and secondary electron spectroscopy [25–32], core level photoelectron spectroscopy [33–37], Auger electron and x-ray fluorescence spectroscopy [38–40], x-ray absorption spectroscopy [41–45], and circularly polarized photoemission [46,47], as well as by theoretical approaches [48–57]. Therefore, we chose graphite as a playground for typical layered materials to study the PSF along the interlayer direction. The interlayer interaction induces the well-known splitting of the π band into two, a lower binding energy band π_L and a higher binding energy band π_H. In the photoelectron spectra, the bands π_L and π_H appear alternatingly in the odd and even BZs along the k_z direction [7–10]. For the explanation of this phenomenon, the dipole selection rules tabulated by Benbow were cited [58], however, this does not give information on the angular distribution nor the disparity of photoelectron intensity among different BZs.

Takizawa *et al.* have measured the photoelectron intensity of graphite in the vicinity of the Fermi level using several different photon energies, and pointed out the importance of the PSF along the k_z axis [5]. Here, we revisited the valence band dispersion of the graphite π band along the k_z axis and measured using a photon energy of 60–230 eV. A 4π-periodic oscillation in the binding energy was clearly observed for the bottom of the π band dispersion during the photon energy scan. We derived an analytic form of PSF and showed that this phenomenon can be understood by considering the constructive and destructive interference of p_z orbitals within the unit cell. The PSF along the k_z direction is also important in the interpretation of the band

dispersion of low-dimensional materials, such as transition metal dichalcogenides, iron pnictide superconductors, and Bi compound topological insulators.

In addition, the inner potential of graphite from the vacuum level was determined to be 17.17 eV. This value roughly corresponds to the midpoint between the bottoms of π and $2s$ bands at the Γ point.

II. THEORETICAL FORMULATION OF PSF

The theoretical formulation of the PSF described elsewhere [2,6] is revised and presented here for extending the discussion. The photoelectron intensity angular distribution $I(\theta,\phi)$ is proportional to the square of the transition matrix element, $\mathbf{M} = \langle f|\mathbf{e}\cdot\mathbf{r}|i\rangle$, between the initial and the final states under the dipole approximation scheme. $\mathbf{G}$ is a reciprocal lattice vector,

$$I(\theta,\phi) \propto D(E_{\mathrm{B}},\mathbf{q})|\mathbf{M}|^2\delta_{E_{\mathrm{f}},h\nu+E_{\mathrm{i}}}\delta_{\mathbf{k},\mathbf{q}+\mathbf{G}}. \quad (1)$$

$D(E_{\mathrm{B}},\mathbf{q})$ is the density of states in a BZ at binding energy E_{B} and at $\mathbf{q}$, i.e., the shape of an isoenergy cross section of the band structure. The two delta functions enforce the energy and momentum conservation laws. Thus, $E_{\mathrm{f}} = h\nu + E_{\mathrm{i}}$ and $\mathbf{G} = \mathbf{k} - \mathbf{q} = \alpha\mathbf{a}^* + \beta\mathbf{b}^* + \gamma\mathbf{c}^*$ (α,β,γ are integer numbers). The dipole operator $\mathbf{e}\cdot\mathbf{r}$ can be expressed using spherical harmonics $Y_{1\mu}(\theta,\phi)$ as $\mathbf{e}\cdot\mathbf{r} = \sqrt{4\pi/3}[e_{-1}Y_{1\bar{1}} + e_0Y_{10} + e_1Y_{11}]$. In the case of $\sigma = 1$ helicity, $e_1 = 1$, $e_0 = 0$, and $e_{-1} = 0$. In the case of x polarization, $e_{\pm 1} = \mp 1/\sqrt{2}$ and $e_0 = 0$.

The initial state $|i\rangle$ having a wave vector $\mathbf{q}$ and energy E_{i} is written as a Bloch state in the tight-binding approximation as

$$|i\rangle = \frac{1}{\sqrt{N}}\sum_j\sum_{n\nu}e^{i\mathbf{q}\cdot(\mathbf{R}_j+\tau_n)}u_{n\nu}(\mathbf{q})\varphi_{n\nu}(\mathbf{r}-\mathbf{R}_j-\tau_n), \quad (2)$$

where N is the total number of atoms, and τ_n is the relative position vector within the jth unit cell at $\mathbf{R}_j$ for the nth atom. $\varphi_{n\nu}(\mathbf{r})$ is the νth orbital of the nth atom, which is the product of a radial function $R(\mathbf{r})$ and a spherical harmonics $Y_{lm}(\theta,\phi)$. $u_{n\nu}(\mathbf{q})$ is its linear combination atomic orbital (LCAO) coefficient.

The final state $|f\rangle$ with the wave vector $\mathbf{k}$ and energy E_{f} can be approximated as a plane wave at the detector in the (θ',ϕ') direction. It is connected to a wave function in the bulk and expanded using an orthogonal set of atomic orbitals $Y_{l'm'}(\theta,\phi)R(\mathbf{r})$ as

$$|f\rangle = 4\pi\sum_{l'm'}i^{l'}e^{-i\delta_{l'}}Y^*_{l'm'}(\theta',\phi')Y_{l'm'}(\theta,\phi)R(\mathbf{r}). \quad (3)$$

Using the above equations for the initial and final states and the dipole perturbation, a formula for matrix elements is derived,

$$\mathbf{M} = \frac{1}{\sqrt{N}}\sum_j\sum_{n\nu}\exp[-i(\mathbf{k}-\mathbf{q})\cdot(\mathbf{R}_j+\tau_n)]u_{n\nu}(\mathbf{q})A_{n\nu}$$

$$= \sum_{n\nu}\exp(-i\mathbf{G}\cdot\tau_n)u_{n\nu}(\mathbf{q})A_{n\nu}. \quad (4)$$

The ADAO, $A_{n\nu} \equiv \langle f|\mathbf{e}\cdot\mathbf{r}|\varphi_{n\nu}\rangle$, is expressed as follows [2],

$$A_{n\nu} = \sum_{l'=l\pm 1}\mathbf{R}_{l'}\sum_{\mu=-1}^{1}e_{\mu}Y_{l'm'}(\theta',\phi')c^1(l',m',l,m). \quad (5)$$

The Gaunt coefficient $c^1(l',m'l,m)$ is nonzero only when $l' - l = \pm 1$ and $\mu = m' - m = \pm 1$ or 0. $\mathbf{R}_{l'}$ is the radial part of the transition matrix element, which is a constant complex number depending on l, l', and photon energy.

When the initial state is composed of only one kind of atomic orbital, C $2p_z$, for example, in the present case, the ADAO term can be separated out of the absolute value as

$$|\mathbf{M}|^2 = |F(\mathbf{k})|^2|A(\theta',\phi')|^2. \quad (6)$$

Finally, the PSF $F(\mathbf{k})$ for one kind of atomic orbital is derived as

$$F(\mathbf{k}) = \sum_n\exp(-i\mathbf{G}\cdot\tau_n)u_n(\mathbf{q}). \quad (7)$$

The term $|F(\mathbf{k})|^2$ is the intensity distribution in reciprocal $\mathbf{k}$ space, which is independent of the energy or the incident angle of the photons. This factor originates from the interference of the photoelectron waves from different atoms in the unit cell and is similar to the structure factors in x-ray or electron diffraction replacing the scattering factors by the coefficients for each atomic orbital in the LCAO wave function.

III. WAVE FUNCTIONS OF π BANDS

Four carbon atoms exist within a unit cell of graphite. The in-plane bonding of carbon has a strong covalent character, namely, σ bonds with sp^2 hybridization. A layer of a honeycomb network structure is formed by sharing the three sp^2 electrons of the three neighboring carbon atoms. The in-plane carbon distance is 1.421 Å. On the other hand, the out-of-plane bonding of carbon is owing to a weak van der Waals interaction produced by the delocalized π orbitals. The interplane spacing of the carbon layers is about 3.35 Å. The carbon layers stack in an ABAB... sequence (Bernal stacking) as shown in Fig. 1(a). Note that there are three- and five-coordinated type carbon atoms.

The four C $2p_z$ orbitals p_{A}, p_{B}, p_{C}, and p_{D} in the unit cell form four π band dispersions. The wave function of the π band
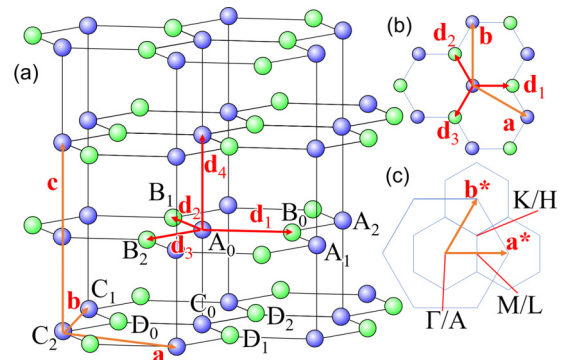

FIG. 1. (a) Structure model, (b) in-plane atomic arrangement, and (c) Brillouin zone of graphite crystal.

$\varphi(\mathbf{q},\mathbf{r})$ is as follows,

$$
\begin{aligned}
\varphi(\mathbf{q},\mathbf{r}) &= \frac{1}{\sqrt{N}} \sum_n e^{i\mathbf{q}\cdot\mathbf{r}_{A_n}} u_A p_A + e^{i\mathbf{q}\cdot\mathbf{r}_{B_n}} u_B p_B \\
&\quad + e^{i\mathbf{q}\cdot\mathbf{r}_{C_n}} u_C p_C + e^{i\mathbf{q}\cdot\mathbf{r}_{D_n}} u_D p_D \\
&= \frac{1}{\sqrt{N}} \sum_n e^{i\mathbf{q}\cdot\mathbf{R}_n} \big[e^{i\mathbf{q}\cdot\mathbf{d}_4/2} \big(u_A p_A + e^{i\mathbf{q}\cdot\mathbf{d}_1} u_B p_B \big) \\
&\quad + e^{-i\mathbf{q}\cdot\mathbf{d}_4/2} \big(u_C p_C + e^{-i\mathbf{q}\cdot\mathbf{d}_1} u_D p_D \big) \big].
\end{aligned}
\tag{8}
$$

$\mathbf{d}_1$, $\mathbf{d}_2$, $\mathbf{d}_3$, and $\mathbf{d}_4$ are the position vectors of the neighboring C atoms shown in Fig. 1. Here, we introduce in-plane and interlayer phase factors,

$$
g(\mathbf{q}) = e^{i\mathbf{q}\cdot\mathbf{d}_1} + e^{i\mathbf{q}\cdot\mathbf{d}_2} + e^{i\mathbf{q}\cdot\mathbf{d}_3},
\tag{9}
$$

$$
h(\mathbf{q}) = e^{i\mathbf{q}\cdot\mathbf{d}_4} + e^{-i\mathbf{q}\cdot\mathbf{d}_4} = 2\cos\mathbf{q}\cdot\mathbf{d}_4.
\tag{10}
$$

The matrix elements $H_{ij} = \langle p_i|H|p_j\rangle$ are classified as follows. Coulomb integrals: $H_{ii} = \epsilon_p$; resonance integrals between two p orbitals in plane (π bond): $H_{AB} = H_{CD} = -V_{pp\pi}$; and perpendicular ($\sigma$ bond): $H_{AC} = V_{pp\sigma}$. According to Harrison, $V_{ppm} = \eta_{ppm}\hbar^2/m_e d^2$, $\hbar^2/m_e = 7.62$ eV Å^2, $\eta_{pp\sigma} = 3.24$, and $\eta_{pp\pi} = -0.81$ [59]. d is the interatomic distance. Hereafter, we write $-V_{pp\pi}$ and $V_{pp\sigma}$ as $+V_\parallel$ and $V_\perp$, respectively. The reported values by Luiggi *et al.* were 2.85 and 0.30 for $V_\parallel$ and $V_\perp$, respectively [60]. The secular equation is

$$
\begin{pmatrix}
\epsilon_p - E & -V_\parallel g & V_\perp h & 0 \\
-V_\parallel g^* & \epsilon_p - E & 0 & 0 \\
V_\perp h & 0 & \epsilon_p - E & -V_\parallel g^* \\
0 & 0 & -V_\parallel g & \epsilon_p - E
\end{pmatrix}
\begin{pmatrix}
u_A \\ u_B \\ u_C \\ u_D
\end{pmatrix} = 0,
\tag{11}
$$

which leads to the following equations for the π bands,

$$
E_{\pi_L} = \epsilon_p - \sqrt{V_\parallel^2|g|^2 + \frac{V_\perp^2|h|^2}{4}} - \frac{V_\perp|h|}{2},
\tag{12}
$$

$$
E_{\pi_H} = \epsilon_p - \sqrt{V_\parallel^2|g|^2 + \frac{V_\perp^2|h|^2}{4}} + \frac{V_\perp|h|}{2}.
\tag{13}
$$

The LCAO coefficients for the π bands (π_H and π_L) are as follows: $u_A = \pm u_C \propto \epsilon_p - E$, $u_B \propto V_\parallel g^*$, and $u_D \propto \pm V_\parallel g$. $u_A^2 + u_B^2 + u_C^2 + u_D^2 = 1$. Along the Γ-A symmetry line where $V_\perp|h|/2V_\parallel|g| \ll 1$, the energy E_π can be approximated using the binominal expansion as follows,

$$
E_{\pi_L} \approx \epsilon_p - V_\parallel|g| - \frac{1}{2}V_\perp|h| - \frac{1}{8}\frac{V_\perp^2|h|^2}{V_\parallel|g|},
\tag{14}
$$

$$
E_{\pi_H} \approx \epsilon_p - V_\parallel|g| + \frac{1}{2}V_\perp|h| - \frac{1}{8}\frac{V_\perp^2|h|^2}{V_\parallel|g|}.
\tag{15}
$$

Note that $\epsilon_p - V_\parallel|g|$ and $\epsilon_p + V_\parallel|g|$ correspond to the binding energy of the π and π^* band dispersions for graphene, respectively. The third term $\pm V_\perp|h|/2$ represents the further splitting of the π and π^* bands. Along the K-H symmetry line where $|g|$ is equal to 0, $E_{\pi_L} = \epsilon_p - V_\perp|h|$ and $E_{\pi_H} = \epsilon_p$.

The PSF for each band is obtained by substituting the coefficients u_n in Eq. (7). The following equation is for the PSF for the π bands. Plus and minus signs correspond to H
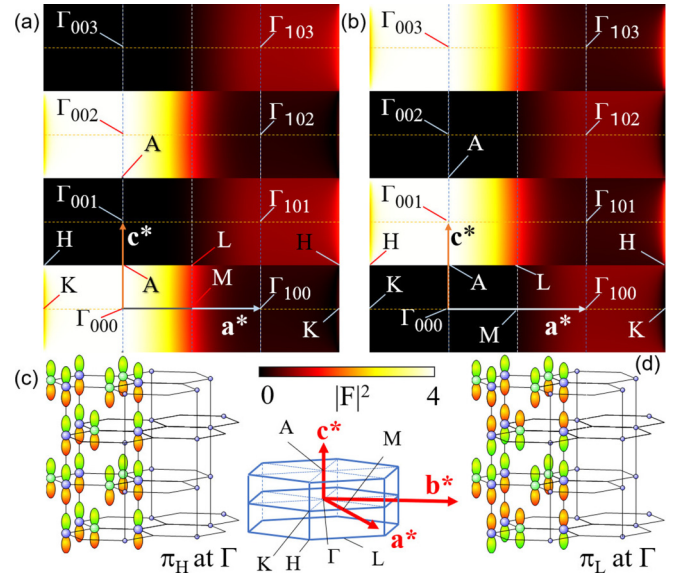

FIG. 2. Square of structure factors (PSF), $|F|^2$, for (a) π_H band and (b) π_L band. C $2p_z$ atomic orbitals at Γ for (c) π_H and (d) π_L bands are shown.

and L bands, respectively,

$$
\begin{aligned}
F &= e^{-\frac{i}{2}\mathbf{G}\cdot\mathbf{d}_4}(u_A + e^{-i\mathbf{G}\cdot\mathbf{d}_1}u_B) \\
&\quad \pm e^{\frac{i}{2}\mathbf{G}\cdot\mathbf{d}_4}(u_C + e^{i\mathbf{G}\cdot\mathbf{d}_1}u_D).
\end{aligned}
\tag{16}
$$

We finally obtain the PSF formula for graphite. Note that $\mathbf{G}\cdot\mathbf{d}_1 = 2\pi(2\alpha + \beta)/3$. For even BZs ($\gamma = 2n$, n is the integer),

$$
|F_{\pi_L}|^2 = \frac{2\big[V_\parallel \sum_{x=1}^3 \sin(\mathbf{G}\cdot\mathbf{d}_1 + \mathbf{q}\cdot\mathbf{d}_x)\big]^2}{(\epsilon_p - E_{\pi_L})^2 + V_\parallel^2 gg^*},
\tag{17}
$$

$$
|F_{\pi_H}|^2 = \frac{2\big[\epsilon_p - E_{\pi_H} + V_\parallel \sum_{x=1}^3 \cos(\mathbf{G}\cdot\mathbf{d}_1 + \mathbf{q}\cdot\mathbf{d}_x)\big]^2}{(\epsilon_p - E_{\pi_H})^2 + V_\parallel^2 gg^*}.
\tag{18}
$$

For odd BZs ($\gamma = 2n + 1$, n is the integer),

$$
|F_{\pi_L}|^2 = \frac{2\big[\epsilon_p - E_{\pi_L} + V_\parallel \sum_{x=1}^3 \cos(\mathbf{G}\cdot\mathbf{d}_1 + \mathbf{q}\cdot\mathbf{d}_x)\big]^2}{(\epsilon_p - E_{\pi_L})^2 + V_\parallel^2 gg^*},
\tag{19}
$$

$$
|F_{\pi_H}|^2 = \frac{2\big[V_\parallel \sum_{x=1}^3 \sin(\mathbf{G}\cdot\mathbf{d}_1 + \mathbf{q}\cdot\mathbf{d}_x)\big]^2}{(\epsilon_p - E_{\pi_H})^2 + V_\parallel^2 gg^*}.
\tag{20}
$$

Figures 2(a) and 2(b) show the PSF for the π_H band and π_L band, respectively. C $2p_z$ atomic orbitals at the Γ point for π_H and π_L bands are depicted together as Figs. 2(c) and 2(d), respectively. Note that the p_z orbitals in the π_L band (bonding) are aligned so that they are antiphase, while the p_z orbitals in the π_H band (antibonding) are aligned so that they have the same phase. These alignments in the π_L and π_H bands make a destructive and constructive interference, respectively, in the first BZ, while they are vice versa in the second BZ in the k_z direction.
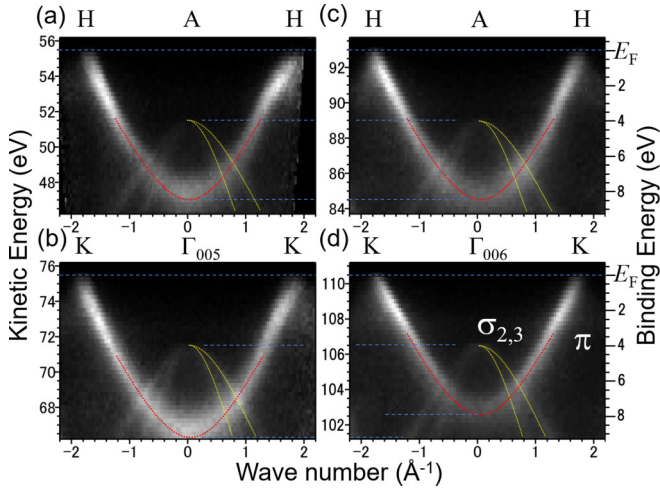
FIG. 3. Graphite π band dispersion measured by angle-resolved photoelectron spectroscopy. The photon energy was (a) 60.0, (b) 80.0, (c) 97.6, and (d) 115.1 eV.

IV. EXPERIMENT

A graphite single crystal of 1 mm diameter was mounted on a sample holder and cleaved just before introducing it into an ultrahigh vacuum for measurements. The surface quality was checked by low-energy electron diffraction (LEED), Auger electron spectroscopy (AES), and x-ray photoemission spectroscopy (XPS) measurements. The selected area for measurement consist of a single domain. No contamination was detected.

Valence band dispersion as a function of photon energy was measured by a concentric hemispherical analyzer at the polarization variable soft x-ray beamline XA03DA of Swiss Light Source, Switzerland [61]. Linearly polarized soft x rays were used. The analyzer was centered at $60°$ off from incident light. The acceptance angle mode of the analyzer was $\pm 30°$ vertical to the plane including the incident light, its electric vector, and the direction to the center of the analyzer entrance slit. The photon energy was calibrated on the C K edge peak of x-ray absorption spectra at 285.50 eV [43,44], while Batson *et al.* reported a value of 285.38 eV [42].

V. RESULTS AND DISCUSSION

A series of π band dispersion cross sections in the K/H-Γ/A plane was measured at different photon energies. Figure 3 shows some of them at the high symmetric points in reciprocal space. The binding energy of the top of the $\sigma_{2,3}$ bands, indicated by yellow curves, was 4.1 eV from the Fermi level, independent of the excitation energy. On the other hand, the binding energy at the bottom of the π band indicated by red curves differed at the A, Γ_{005}, and Γ_{006} points. It was the largest and the smallest at the Γ_{005} and Γ_{006} points, respectively, while it was in a midvalue at the A points.

The valence band dispersion cross section of graphite along the k_z axis measured using photon energies between 60 and 230 eV is shown in Fig. 4(a). The oscillation in the binding energy was clearly observed for the π band dispersion as a function of photon energy, as indicated by a pink curve.
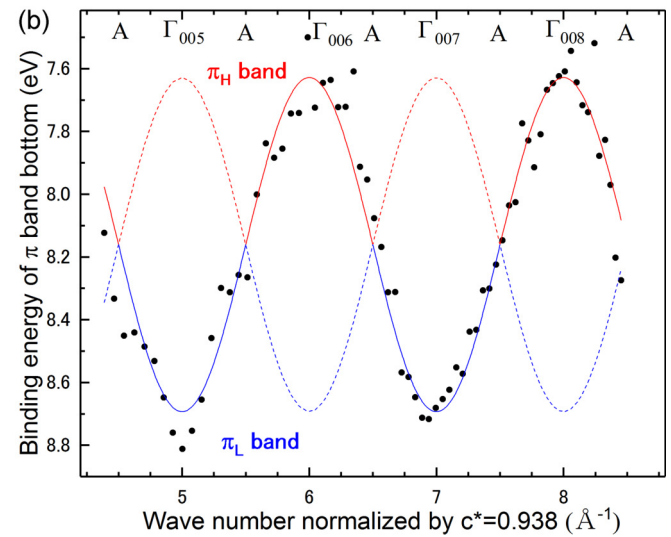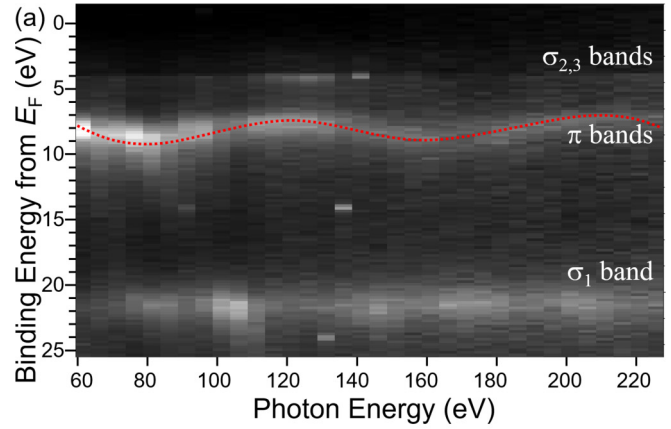

FIG. 4. (a) Graphite band dispersion measured at Γ/A as a function of photon energy. The red curve indicates the oscillation of the π band dispersion. (b) The binding energy of the bottom of the π band dispersion plotted as a function of wave number.

The binding energy of the bottom of π band as a function of photon energy is plotted in Fig. 4(b). The abscissa is the wave number normalized by the reciprocal lattice constant c^*. Integer number positions correspond to the Γ points. The kinetic energy for each data point was converted to the wave number considering the inner potential as a fitting parameter, so that the position of each energy minimum and maximum comes to the Γ point.

At the odd number [$k_z = (2n + 1)c^*$] points, the binding energy of the π band bottom is large, while at the even number [$k_z = 2nc^*$] points, it is small. The former corresponds to the π_L band. The latter corresponds to the π_H band. This oscillation is well explained by the PSF effect along the k_z direction shown in Figs. 2(a) and 2(b). The π_L band is formed by the p_z orbitals aligned in the antiphase, causing destructive interference at the even number Γ_{002n} points. On the other hand, the π_H band is formed by the p_z orbitals aligned with the same phase, causing constructive interference at the even number Γ_{002n} points.

The fitting was done by using the inner potential as well as the binding energy and amplitude of the cosine curve as the fitting parameters so that the energy oscillation maxima

TABLE I. Band energies with respect to the Fermi level at the Γ point of graphite (in eV).

	This work	Previous works by ARPES				
$\sigma_{2,3}$	4.1	4.6 [12]	5.5 [25]	5.3 [13]	4.25 [26]	4.1 [8]
π	7.63	7.2 [12]	6.6 [25]	7.6 [13]	8.1 [26]	7.8 [8]
	8.69	8.1 [12]	8.5 [25]	9.0 [13]	9.3 [26]	9.2 [8]
σ_1	21.6	21.0 [7]			21.7 [14]	21.8 [8]

and minima match with the position of the Γ points. The inner potential of graphite was determined to be 17.17 ± 0.1 eV from the vacuum level. It agrees with the previously reported values of 16.4 [10], 16.5 [62], and 17.25 eV [24], but is larger than the older value of 14.5 eV [7]. It is interesting to note that the few-layer graphene has a similar inner potential [9]. This value roughly corresponds to the midpoint between the bottoms of the π and σ_1 bands at the Γ point (see Table I). Furthermore, the resonance integral between the interlayer p_z orbitals $V_\perp$ was derived as 0.53 eV from this fitting. $V_\parallel$ was determined as 2.72 eV from the in-plane π band dispersion along the A-H symmetry line. Figures 2(a) and 2(b) are the square of PSF calculated based on these values and Eqs. (12) and (13).

The PSF effect leads to the complete disappearance of one π band along the sample surface normal axis [8,32]. There are some measurements reporting the observation of both π_L and π_H band dispersions simultaneously in the vicinity of the K points [10,21], which can be also explained from Figs. 2(a) and 2(b). The breaking of the bulk translational symmetry at the topmost surface layer, the enhancement of the surface sensitivity at low kinetic energy, and the umklapp scattering process at the final state were not taken into account in the present PSF formalism. These may give an additional effect of breaking the 4π-periodic oscillation (see Table I).

VI. CONCLUSION

The valence band dispersion of the graphite π band along the k_z axis was measured using photon energies between 60 and 230 eV. The interlayer interaction induces the well-known splitting of the π band into two, a lower binding energy band π_L and a higher binding energy band π_H. In the photoelectron spectra, the band π_L was detected in the BZs centered at $(2n+1)c^*$, while the band π_H was detected in the BZs centered at $2nc^*$. As a result, an oscillation in binding energy was observed for the bottom of the π band dispersion during a photon energy scan. This phenomenon is well explained by the constructive and destructive interference along the k_z direction, i.e., the PSF effect. The bonding characters of the π bands can be specified by comparing the photoelectron intensity with the calculated PSF. This concept is applicable to the investigation of the electronic structure of various layered materials. Furthermore, the inner potential of graphite was determined to be 17.17 eV from the vacuum level.

[1] H. Daimon, M. Kotsugi, K. Nakatani, T. Okuda, and K. Hattori, Surf. Sci. **438**, 214 (1999).

[2] H. Daimon, S. Imada, H. Nishimoto, and S. Suga, J. Electron Spectrosc. Relat. Phenom. **76**, 487 (1995).

[3] H. Nishimoto, T. Nakatani, T. Matsushita, S. Imada, H. Daimon, and S. Suga, J. Phys.: Condens. Matter **8**, 2715 (1996).

[4] E. L. Shirley, L. J. Terminello, A. Santoni, and F. J. Himpsel, Phys. Rev. B **51**, 13614 (1995).

[5] M. Takizawa, H. Namba, F. Matsui, and H. Daimon, J. Electron Spectrosc. Relat. Phenom. **181**, 193 (2010).

[6] F. Matsui, T. Matsushita, and H. Daimon, J. Electron Spectrosc. Relat. Phenom. **195**, 347 (2014).

[7] A. R. Law, M. T. Johnson, and H. P. Hughes, Phys. Rev. B **34**, 4289 (1986).

[8] T. Kihlgren, T. Balasubramanian, L. Walldén, and R. Yakimova, Phys. Rev. B **66**, 235422 (2002).

[9] T. Ohta, A. Bostwick, J. L. McChesney, T. Seyller, K. Horn, and E. Rotenberg, Phys. Rev. Lett. **98**, 206802 (2007).

[10] A. Grüneis, C. Attaccalite, T. Pichler, V. Zabolotnyy, H. Shiozawa, S. L. Molodtsov, D. Inosov, A. Koitzsch, M. Knupfer, J. Schiessling, R. Follath, R. Weber, P. Rudolf, L. Wirtz, and A. Rubio, Phys. Rev. Lett. **100**, 037601 (2008).

[11] F. R. McFeely, S. P. Kowalczyk, L. Ley, R. G. Cavell, R. A. Pollak, and D. A. Shirley, Phys. Rev. B **9**, 5268 (1974).

[12] W. Eberhardt, I. T. McGovern, E. W. Plummer, and J. E. Fischer, Phys. Rev. Lett. **44**, 200 (1980).

[13] D. Marchand, C. Frétigny, M. Laguës, F. Batallan, Ch. Simon, I. Rosenman, and R. Pinchaux, Phys. Rev. B **30**, 4788 (1984).

[14] C. Heske, R. Treusch, F. J. Himpsel, S. Kakar, L. J. Terminello, H. J. Weyer, and E. L. Shirley, Phys. Rev. B **59**, 4680 (1999).

[15] F. Matsui, Y. Hori, H. Miyata, N. Suganuma, H. Daimon, H. Totsuka, K. Ogawa, T. Furukubo, and H. Namba, Appl. Phys. Lett. **81**, 2556 (2002).

[16] K. Sugawara, T. Sato, S. Souma, T. Takahashi, and H. Suematsu, Phys. Rev. B **73**, 045124 (2006).

[17] T. Ohta, A. Bostwick, T. Seyller, K. Horn, and E. Rotenberg, Science **313**, 951 (2006).

[18] K. Sugawara, T. Sato, S. Souma, T. Takahashi, and H. Suematsu, J. Phys. Chem. Solids **69**, 2996 (2008).

[19] C. S. Leem, C. Kim, S. R. Park, M.-K. Kim, H. J. Choi, C. Kim, B. J. Kim, S. Johnston, T. Devereaux, T. Ohta, A. Bostwick, and E. Rotenberg, Phys. Rev. B **79**, 125438 (2009).

[20] R. Kundu, P. Mishra, B. R. Sekhar, M. Maniraj, and S. R. Barman, Physica B **407**, 827 (2012).

[21] S. Tanaka, M. Matsunami, and S. Kimura, Phys. Rev. B **84**, 121411 (2011).

[22] S. K. Mahatha and K. S. R. Menon, Surf. Sci. **606**, 1705 (2012).

[23] S. Pagliara, M. Montagnese, S. Dal Conte, G. Galimberti, G. Ferrini, and F. Parmigiani, Phys. Rev. B **87**, 045427 (2013).

[24] C.-M. Cheng, C.-J. Hsu, J.-L. Peng, C.-H. Chen, J.-Y. Yuh, and K.-D. Tsuei, Appl. Surf. Sci. **354**, 229 (2015).

[25] A. R. Law, J. J. Barry, and H. P. Hughes, Phys. Rev. B **28**, 5332 (1983).

[26] T. Takahashi, H. Tokailin, and T. Sagawa, Phys. Rev. B **32**, 8317 (1985).

[27] B. Reihl, J. K. Gimzewski, J. M. Nicholls, and E. Tosatti, Phys. Rev. B **33**, 5770 (1986).

[28] I. Schäfer, M. Schlüter, and M. Skibowski, Phys. Rev. B **35**, 7663 (1987).

[29] F. Maeda, T. Takahashi, H. Ohsawa, S. Suzuki, and H. Suematsu, Phys. Rev. B **37**, 4482 (1988).

[30] V. N. Strocov, P. Blaha, H. I. Starnberg, M. Rohlfing, R. Claessen, J.-M. Debever, and J.-M. Themlin, Phys. Rev. B **61**, 4994 (2000).

[31] V. N. Strocov, A. Charrier, J.-M. Themlin, M. Rohlfing, R. Claessen, N. Barrett, J. Avila, J. Sanchez, and M.-C. Asensio, Phys. Rev. B **64**, 075105 (2001).

[32] N. Barrett, E. E. Krasovskii, J.-M. Themlin, and V. N. Strocov, Phys. Rev. B **71**, 035427 (2005).

[33] R. A. P. Smith, C. W. Armstrong, G. C. Smith, and P. Weightman, Phys. Rev. B **66**, 245409 (2002).

[34] F. Matsui, H. Daimon, F. Z. Guo, and T. Matsushita, Appl. Phys. Lett. **85**, 3737 (2004).

[35] M. R. C. Hunt, Phys. Rev. B **78**, 153408 (2008).

[36] S. Lizzit, G. Zampieri, L. Petaccia, R. Larciprete, P. Lacovig, E. D. L. Rienks, G. Bihlmayer, A. Baraldi, and P. Hofmann, Nat. Phys. **6**, 345 (2010).

[37] F. Matsui, T. Matsushita, and H. Daimon, J. Phys. Soc. Jpn. **81**, 114604 (2012).

[38] M. A. Smith and L. L. Levenson, Phys. Rev. B **16**, 2973 (1977).

[39] J. A. Carlisle, E. L. Shirley, E. A. Hudson, L. J. Terminello, T. A. Callcott, J. J. Jia, D. L. Ederer, R. C. C. Perera, and F. J. Himpsel, Phys. Rev. Lett. **74**, 1234 (1995).

[40] L. Calliari, G. Speranza, and A. Santoni, J. Electron Spectrosc. Relat. Phenom. **127**, 125 (2002).

[41] D. A. Fischer, R. M. Wentzcovitch, R. G. Carr, A. Continenza, and A. J. Freeman, Phys. Rev. B **44**, 1427 (1991).

[42] P. E. Batson, Phys. Rev. B **48**, 2608 (1993).

[43] P. Skytt, P. Glans, D. C. Mancini, J.-H. Guo, N. Wassdahl, J. Nordgren, and Y. Ma, Phys. Rev. B **50**, 10457 (1994).

[44] D. Pacilé, M. Papagno, A. Fraile Rodríguez, M. Grioni, L. Papagno, C. Ö. Girit, J. C. Meyer, G. E. Begtrup, and A. Zettl, Phys. Rev. Lett. **101**, 066806 (2008).

[45] R. Ahuja, P. A. Brühwiler, J. M. Wills, B. Johansson, N. Mårtensson, and O. Eriksson, Phys. Rev. B **54**, 14396 (1996).

[46] H. Daimon, Phys. Rev. Lett. **86**, 2034 (2001).

[47] F. Matsui, T. Matsushita, Y. Kato, F. Z. Guo, and H. Daimon, J. Phys. Soc. Jpn. **76**, 013705 (2007).

[48] P. R. Wallace, Phys. Rev. **71**, 622 (1947).

[49] J. W. McClure, Phys. Rev. **108**, 612 (1957).

[50] G. S. Painter and D. E. Ellis, Phys. Rev. B **1**, 4747 (1970).

[51] R. C. Tatar and S. Rabii, Phys. Rev. B **25**, 4126 (1982).

[52] H. J. F. Jansen and A. J. Freeman, Phys. Rev. B **35**, 8207 (1987).

[53] J.-C. Charlier, X. Gonze, and J.-P. Michenaud, Phys. Rev. B **43**, 4579 (1991).

[54] J.-C. Charlier, J.-P. Michenaud, and X. Gonze, Phys. Rev. B **46**, 4531 (1992).

[55] J. C. Boettger, Phys. Rev. B **55**, 11202 (1997).

[56] E. L. Shirley, Phys. Rev. B **54**, 16464 (1996).

[57] B. Partoens and F. M. Peeters, Phys. Rev. B **74**, 075404 (2006).

[58] R. L. Benbow, Phys. Rev. B **22**, 3775 (1980).

[59] W. A. Harrison, *Electronic Structure and the Properties of Solid*s (W. H. Freeman and Company, San Francisco, 1980).

[60] N. J. Luiggi and W. Barreto, Phys. Rev. B **34**, 2863 (1986).

[61] M. Muntwiler, J. Zhang, R. Stania, F. Matsui, P. Oberta, U. Flechsig, L. Patthey, C. Quitmann, T. Glatzel, R. Widmer, E. Meyer, T. A. Jung, P. Aebi, R. Fasel, and T. Greber, J. Synchrotron Radiat. **24**, 354 (2017).

[62] S. Y. Zhou, G. H. Gweon, and A. Lanzara, Ann. Phys. (NY) **321**, 1730 (2006).